GEOPHYSICAL MONOGRAPH SERIES VOL. 14
The Structure and Physical Properties of the Earth's Crust
Edited by John G. Heacock
AMERICAN GEOPHYSICAL UNION
Washington, D. C. 20037

Crustal Investigations by the Magnetotelluric Tensor Impedance Method

D. R. WORD, H. W. SMITH, AND F. X. BOSTICK, JR.

Electrical Engineering Department, The University of Texas at Austin
Austin, Texas 78712

Abstract. A magnetotelluric (MT) sounding method that involves a tensor impedance relationship between the surface electric and magnetic micropulsation fields of the earth has been developed. The role of the tensor impedance, including the vertical magnetic field relationship, is discussed. MT soundings made at 7 sites along a sixty-mile traverse east of Austin, Texas, in the frequency band 10^{-4} to 10 Hz are analyzed. The traverse bears northwest-southeast and crosses the Ouachita fold belt system on the flanks of the Llano uplift. The sounding covers the approximate depth range of 0.1 to 100 km. An earth model is derived from the sounding and includes a vertical cross section of the estimated conductivity distribution and estimates of the strike directions of the various formations represented by the cross section. The model is compared with available geological information, and an attempt is made to explain some of the observed three-dimensional properties of the impedance function. The model is in good agreement with expected geology to depths for which surface and borehole data can be reasonably extrapolated. The sounding responds to materials ranging from Cretaceous sediments through the upper mantle and provides reasonable definition of a high-resistivity region which appears to be the Precambrian granite basement. Along the traverse, the top of this basement occurs at depths ranging from 3 to 10 km. In the upper mantle, a resistivity decrease to about 1 Ω-m or less is found to occur at depths of about 60 to 100 km. An apparent northwesterly rise in the conductive substrate is found. This and other evidence seems to suggest an uplift in the conductive mantle in association with the Llano uplift.

Southeast of the Llano uplift in central Texas, the Precambrian granite dips sharply toward the Gulf coast beneath a thickening overburden of sedimentary rocks. The surface of the granite basement becomes indeterminable within a few tens of miles from its outcrop in Llano County. An MT survey along a traverse extending from near a point of outcrop southeastward toward the coast was performed for two purposes.

The first purpose was to extend the known depths to the granite basement beyond the boundaries within which it was defined by borehole penetrations. It was reasoned that the Precambrian material would, on the average, be more resistive than the sedimentary rocks, so that a sharp contrast in the electrical resistivity would occur at the base of the sediments. Such an interface, as well as other significant conductivity features both within and below the sediments, should be defined by the MT survey.

The second purpose of the study was to apply and evaluate the tensor-impedance method of MT analysis to data acquired over reasonably well known inhomogeneous geologic structures. The Ouachita fold belt and the overlying sediments provide such structures in the sedimentary rocks beneath the survey path. The Ouachita system is a major Paleozoic orogenic belt of severely folded and faulted Paleozoic rocks that has several borehole penetrations in the frontal zone near the Llano uplift. The inhomogeneity of the lithology in this system leads one to suspect corresponding inhomogeneities in the electrical conductivity. The Ouachita system is overlain by Cretaceous and younger sediments within which the lithological units are fairly planar and dip southeastward. Electric well logs indicate a corresponding tendency toward stratification of the electrical conductivity.

In his original discussion of the magnetotelluric method of subsurface resistivity sounding, *Cagniard* [1953] assumed that the conductive earth is horizontally stratified and is illuminated by plane electromagnetic waves propagating

vertically downward. The frequent failure of this model to explain the measured data and to produce repeatable results has brought about two main criticisms. The first of these was directed at the source assumption, and the second was directed at the one-dimensional earth model.

Regarding the source, *Wait* [1954], *Price* [1962], and *Srivastava* [1965] discussed the effects of horizontal variations in the primary fields due to limited spatial dimensions of the source. They pointed out that field variations must be small over a lateral distance comparable to a skin depth in the conductive earth at the frequency of concern. The degree of source effect is still in question and possibly is considerable at times and in some situations, especially at high latitudes where the source amplitude for some frequency bands is usually much larger and peaked near the auroral zone [see, for example, *McNish*, 1964; *Heirtzler*, 1964], where large lateral gradients might become significant. However, empirical measurements and coherence analyses of micropulsation signals at widely separated stations [*Bloomquist et al.*, 1967; *Orange and Bostick*, 1965; *Swift*, 1967], as well as theoretical source studies [*Prince et al.*, 1964], lend credence to the assumption of large source dimensions for low and middle latitudes, often of continental extent or greater. Based on this evidence, the effects of finite source dimensions were ignored in this study. This omission is undoubtedly responsible for some of the mild scatter in the processed MT data.

Of more direct concern here is the question of a multidimensional earth model. The scalar impedance described by Cagniard for his one-dimensional earth model is inadequate for the interpretation of lateral inhomogeneities or anisotropies in the conductive earth. The result of these spatial irregularities is that the electric and magnetic fields at the earth's surface are no longer orthogonal. *Cantwell* [1960] suggested that the tangential fields can be related in general by a two-dimensional tensor quantity that relates each electric-field component to the total tangential magnetic field. *Bostick and Smith* [1962] also recognized the tensor nature of the surface impedance and demonstrated the behavior with axis rotation; they pointed out means for determining the apparent strike of an earth anomaly from the principal direction of

A considerable amount of experimental MT evidence has been reported since the Cagniard theory was first proposed [*Bostick and Smith*, 1961; *Bryunelli*, 1964; *Cantwell and Madden*, 1960; *Fournier*, 1963; *Hopkins and Smith*, 1966; *Parkinson*, 1962; *Pokityanski*, 1961; *Popeyev*, 1965; *Spitznogle*, 1966; *Srivastava et al.*, 1963; *Swift*, 1967; *Vozoff et al.*, 1963, 1964]; however, many of the questions and problems involved, particularly with interpretive methods, still remain. To date, there has been reported only limited experimental evidence using the tensor impedance method.

Interpretation of the MT tensor impedance, once it has been measured, needs further study. Analytical solutions for three-dimensional geometries are almost non-existent and unobtainable with present methods. Analog solutions are feasible, but they are usually cumbersome and are seldom attempted. Consequently, interpretation has been limited to two-dimensional geometries. Approximate analytical solutions have been obtained for a few simple two-dimensional models such as the vertical plane contact or the dike [*d'Erceville and Kunetz*, 1962; *Rankin*, 1962; *Weaver*, 1963] and the small-amplitude sinusoidal horizontal interface [*Mann*, 1964]. Numerical solutions can be generated for almost any two-dimensional model [*Patrick*, 1969], but there is an obvious need for improvement in interpretive techniques for three-dimensional geometries. Three dimensionality in earth structure is readily identified in the measured impedance [*Swift*, 1967; *Sims*, 1969], but thus far the resulting data have only been rejected and not interpreted.

The vertical magnetic field is of considerable importance. Its linear relationship with tangential fields has been known for some time [*Bryunelli*, 1964; *Parkinson*, 1962] as well as its potential for determining strike direction in the anomaly, especially in connection with the seacoast effect [*Weaver*, 1963]. However, it has not been used to any extent in interpreting MT soundings.

THEORY

For the analytical model used here in the interpretation of the MT data, the conductive earth is assumed to occupy the half space $z \geq 0$, as shown in Figure 1*b*. Unless otherwise noted, lateral coordinates x and y is north and east, respectively. The half space $z < 0$ is considered to be free space. Electromagnetic excitation is assumed to be provided by plane waves propagating vertically downward; this assumption eliminates the vertical components of the electric and magnetic fields from the primary waves. Secondary fields caused by reflections from lateral variations in the conductivity of the earth are the only source of the vertical components of the electromagnetic fields.

The MT analysis involves the estimation of various relationships between the Fourier resolved electromagnetic field components measured at the earth's surface. The vertical and two orthogonal horizontal components of the magnetic field plus two orthogonal horizontal components of the electric field constitute the set of field components measured at each site for this study. The vertical field in the air space above the earth was not measured, because it is strongly affected by static atmospheric electricity at the relatively low MT frequencies, nor was an attempt made to measure the vertical field just within the surface of the conductive earth. At the low frequencies involved in the MT study, displacement currents within the conductive earth may be neglected in favor of the conduction currents. Consequently, there is very little vertical component of current density and thus of vertical electric field within the conductive earth just beneath the surface. Since all the measured components of the electromagnetic field are continuous at the earth's surface, it is necessary to measure them only near the interface on either side.

The frequency domain relations between the Fourier resolved tangential components of the surface electromagnetic fields are written as

$$[E] = [Z][H] \tag{1}$$

where

$$[E] = \begin{bmatrix} E_x \\ E_y \end{bmatrix}$$

and

$$[H] = \begin{bmatrix} H_x \\ H_y \end{bmatrix}$$

are the column vectors representing the tangential electric and magnetic field vectors, respectively, and

$$[Z] = \begin{bmatrix} Z_{xx} & Z_{xy} \\ Z_{yx} & Z_{yy} \end{bmatrix}$$

is the rank two tensor impedance.

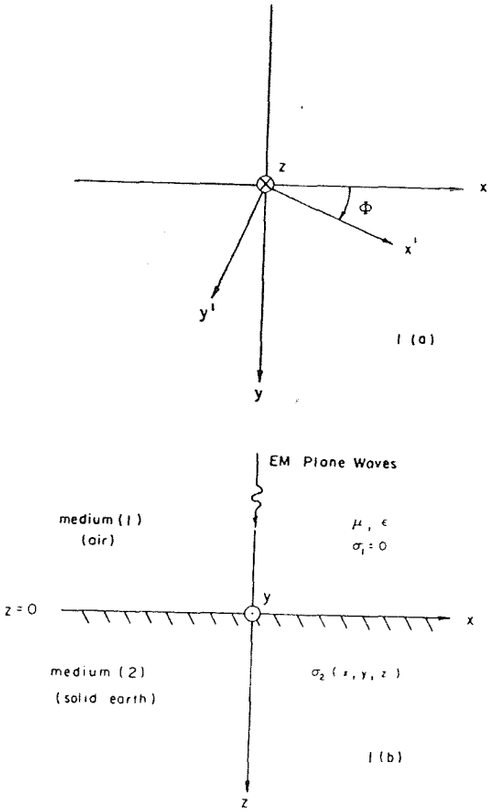

Fig. 1. Coordinate system and earth model.

It is assumed that, if (1) were derived for some arbitrary earth model, the impedance elements would be a function of position, the source field configuration and, of course, the frequency. For an example of the source dependence, see *Wait* [1954], in which the nature of a scalar impedance estimate that is derived for a homogeneous isotropic earth model with a complex source distribution is examined. It is further assumed here that, since the source fields are geomagnetic micropulsations and since the spatial configuration of these fields varies with time, the depen-

dence of the impedance elements on the source is reflected as a time variation of the elements themselves. The experimental estimates of the impedance elements obtained along the central Texas traverse do vary from one data sample to another, but this variation is relatively small except at the very lowest recorded frequencies. It is assumed that this temporal stability of the estimates indicates that they are only a slight function of the configuration of the source fields having the spatial extent of the geomagnetic micropulsations. This is not to say that the total micropulsation fields are uniform over any large area. On the contrary, the total fields, including both the relatively uniform source or incident fields and the possibly complex reflected fields, may have rather large spatial derivatives producing the functional dependence of the impedance estimates on position. For the remainder of this paper, the dependence of the impedance elements on the character of the source is suppressed.

Subject to the same considerations concerning the source, the vertical component of the magnetic field, H_z, can be related to the tangential electric field components with the expression

$$[H_z] = [Y_z][E] \tag{2}$$

where

$$[Y_z] = [Y_{zx}\, Y_{zy}]$$

is a tensor admittance function.

Both $[Z]$ and $[Y_z]$ are estimated from the measured field data and are used for the purpose of constructing an interpretational model. All six elements of the combined tensors $[Z]$ and $[Y_z]$ can be estimated from two independent time sequences of the recorded field components or, effectively, from two different polarizations of the source field [*Sims*, 1969].

Rotation of coordinates. If $[\eta]$ is the coordinate rotation matrix for a vector in the xy plane, then in the primed coordinates of Figure 1*a*, rotated clockwise by the angle Φ,

$$[Z'] = [\eta][Z][\eta]^{-1} \tag{3}$$

The loci of the $[Z'(\Phi)]$ elements in the complex impedance plane as a function of rotation angle Φ are generally elliptical, as recognized by *Sims* [1969], who suggests the graphical representation of Figure 2, showing the impedance behavior with rotation. Here, the ellipses are the loci of the impedance element phasors. All ellipses for the $[Z']$ element have the same dimensions and orientation. The ellipses for Z_{xy}', Z_{yx}', and Z_{xx}' are centered at $\pm Z_1$ and Z_2, respectively, as shown in Figures 2*a* and 2*b*. Z_1 and Z_2 are invariant with axis rotation. Z_3 is the value of the major axis, and Z_4 is the minor axis for each ellipse. The impedance loci have a rotation period of 180° in Φ. With Φ_0 as defined in Figure 2, the major and minor axis intercepts correspond to the angles $\Phi = \Phi_0 \pm n\,45°$

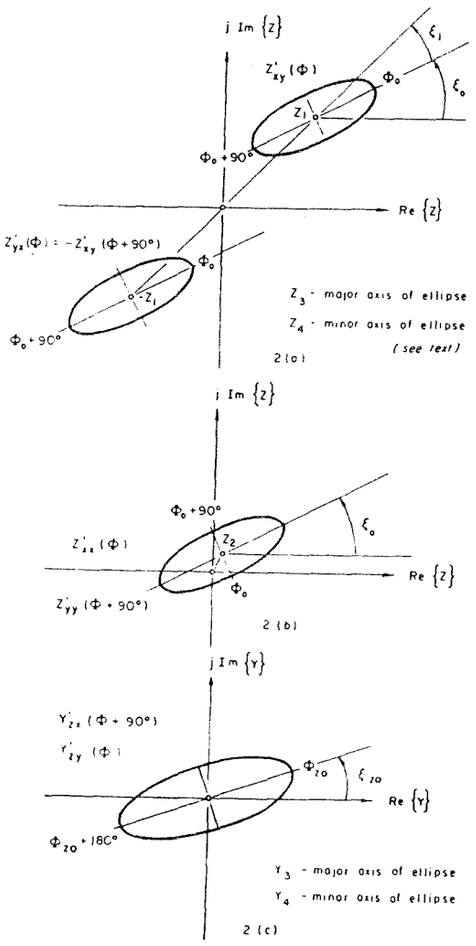

Fig. 2. Loci of impedance and admittance elements in the complex plane with respect to rota-

Complex plane loci for $[Y_z'(\Phi)]$ are also elliptical, in general, as illustrated in Figure 2*c*. For a given frequency, the ellipse is centered on the origin, and the angle between the major axis of the ellipse and the real axis is designated as ξ_{z0}. Y_3 and Y_4 are the values of the major and minor axes, respectively. The rotation period for these loci is 360° in Φ, and the major and minor axes correspond to $\Phi = (\Phi_{z0} \pm n\,90°)$ $n = 0, 1, 2, \cdots$, where Φ_{z0} is as defined in the figure.

One-dimensional earth. When the earth conductivity is a function of z only, the surface impedance is representable as a complex scalar $Z_s = Z_1$ that is invariant with Φ, and the elements of $[Z']$ become

$$Z_{xx}' = Z_{yy}' = 0 \tag{4a}$$

$$Z_{xy}' = -Z_{yx}' = Z_s \tag{4b}$$

for all Φ. The rotation loci for $[Z']$ elements are thus point ellipses in the complex plane centered at the origin and $\pm Z_s$.

There is no vertical magnetic field, $H_z = 0$, so that the rotation loci for elements of $[Y_z']$ are point ellipses centered at the origin.

Two- and three-dimensional earth. Arbitrary conductivity structures usually produce elements of $[Z']$ and $[Y_z']$ whose rotational loci are characterized by the open ellipses shown in Figure 2. Suppose, however, that there exists a vertical plane of symmetry through the measuring point (i.e., a plane containing the z axis, about which the structures on either side are mirror images of each other); this also includes the possibility of a two-dimensional earth as a special case. As the coordinate $x'y'$ axes are rotated, the tensor $[Z']$ must diagonalize whenever the x' axis or the y' axis lies within the plane of symmetry (i.e., for 90° increments of Φ) [*Word et al.*, 1970] such that

$$\begin{aligned} &Z_{xx}'(\Phi) = Z_{yy}'(\Phi) = 0 \qquad \Phi = \Phi_0 \pm n90° \\ &Z_{xx}'(\Phi) = -Z_{yy}'(\Phi) \qquad \Phi \neq \Phi_0 \pm n90° \end{aligned} \tag{5}$$

where $n = 0, 1, 2, \cdots$. This causes the rotation loci for Z_{xx}' and Z_{yy}' to be a straight line ellipse centered on the origin. The loci for Z_{xy}' and Z_{yx}' are straight line ellipses also and are centered at $\pm Z_1$.

The vertical magnetic field H_z may or may not

In any case, each element of $[Y_z']$ must vanish for some value of $\Phi = \Phi_1$ and for $\Phi_1 + 180°$. This requires that the loci be in general straight-line ellipses centered on the origin. For a two-dimensional structure, the x' axis is aligned with the plane of symmetry for $\Phi = \Phi_{z0}$ and defines the characteristic dip direction of the structure. Note that for a two-dimensional or symmetrical structure the angle Φ_{z0} is a function of geometry only and is thus a useful diagnostic parameter.

In summary, the various conditions relating to axis rotation are the following.

For earth conductivity $\sigma_2(x, y, z)$ arbitrary, rotation loci must be primarily elliptical, as pictured in Figures 2*a*, 2*b*, and 2*c*.

For earth conductivity $\sigma_2(x, y, z)$ symmetrical about some vertical plane of symmetry, first, $[Z'(\Phi)]$ must and can only diagonalize for 90° increments in Φ. Rotation loci are line ellipses centered at the origin and $\pm Z_1$. Second, $[Z'(\Phi)]$ must diagonalize when the x' axis or y' axis is within the plane of symmetry. Third, $[Y_z']$ elements each must and can only vanish at 180° increments in Φ. Rotation loci are line ellipses centered at the origin. Fourth, an element of $[Y_z']$ must vanish whenever the x' axis or the y' axis lies within the plane of symmetry.

For earth conductivity $\sigma_2(x, y, z) = \sigma_2(z)$, rotation loci for $[Z']$, $[Y_z']$ are all point ellipses centered at the origin and $\pm Z_1$.

Three-dimensionality indicators. Precise interpretation of the two-dimensional tensor impedance $[Z]$ is limited at best to two-dimensional or simpler geometry. Some parameters can be defined that indicate departure from two-dimensionality; they thus serve as guidelines for interpretation.

The 'skew' index as defined by *Swift* [1967] is given by

$$\alpha \equiv \frac{(Z_{xx}' + Z_{yy}')}{(Z_{xy}' - Z_{yx}')} = \frac{Z_2}{Z_1} \tag{6}$$

The index α is invariant with Φ. It may be noted that α is the ratio of the displacements of the centers from the origin of the rotational ellipses for the diagonal and cross tensor impedance elements. The condition $|\alpha| = 0$ is a

sionality, since it requires only that the Z_{xx}', Z_{yy}' loci be centered on the origin.

Another indication of three dimensionality is the eccentricity of the loci ellipse for $[Z'(\Phi)]$. Consider the parameter defined as

$$\beta(\Phi) = \frac{(Z_{xx}' - Z_{yy}')}{(Z_{xy}' + Z_{yx}')} \tag{7}$$

If the rotation loci are line ellipses, then the numerator must vanish for some $\Phi = \Phi_0$ and, thus, $\beta(\Phi_0) = 0$ for a two-dimensional earth. It is easily shown by substitution of (3) that $(Z_{xx}' - Z_{yy}')$ and $(Z_{xy}' + Z_{yx}')$ of Figure 2 must be in time phase in order for $\beta(\Phi_0)$ to vanish. Therefore, $\beta(\Phi)$ is real for a two-dimensional earth and complex in general for a three-dimensional earth. The 'ellipticity index' [*Sims*, 1969], defined as

$$\beta_0 \equiv \beta(\Phi_0) = Z_4/Z_3 \tag{8}$$

is the ratio of minor to major axes of the impedance ellipse. A nonzero value for $|\beta_0|$ is indicative of three dimensionality.

The condition

$$|\alpha| = 0 \qquad |\beta_0| = 0 \tag{9}$$

is a necessary and sufficient condition for two dimensionality that is used here to mean that $[Z'(\Phi)]$ is antisymmetric and will diagonalize for some value of Φ.

As the three-dimensional effect becomes small, it is possible for the axes of the rotation ellipse to become vanishingly small compared to the elements of $[Z']$, and this must be considered in judging the degree of three dimensionality. It might be desirable to weight the importance of β_0 as

$$\beta_{00} \equiv \beta_0 \frac{(Z_{xy}' + Z_{yx}')}{(Z_{xy}' - Z_{yx}')|_{(\Phi=\Phi_0)}} = \frac{(Z_{xx}' - Z_{yy}')}{(Z_{xy}' - Z_{yx}')|_{(\Phi=\Phi_0)}} \tag{10}$$

Ellipticity indices can also be defined for $[Y_s']$ in a similar manner. If

$$\beta_{s0} \equiv \beta_s(\Phi_{s0}) = \left.\frac{Y_{xx}'}{Y_{xy}'}\right|_{(\Phi=\Phi_{s0})} \tag{11}$$

$|\beta_{s0}|$ is zero for an apparent two dimensionality but is not necessarily nonzero for an apparent

Interpretation technique. MT interpretation is based primarily on the point relationships:

$$[E] = [Z][H] \tag{12a}$$

$$[H_s] = [Y_s][E] \tag{12b}$$

which ideally would be known as a function of x and y as well as frequency.

The most practical approach to MT interpretation is to first synthesize a 'best' one-dimensional conductivity distribution $\sigma(z)$ from the tensor impedance $[Z]$ at each data site. A set of $\sigma(z)$ models for a grid of data sites can then be contoured or otherwise assembled to produce an initial estimate of the three-dimensional structure. Two- and three-dimensional model solutions are of little value at the outset, at least on a trial-and-error basis, but they serve more appropriately as a means of verification and refinement of the initial interpretation. Further refinement of the earth model can hopefully be accomplished by considering the coordinate rotation properties of $[Z]$ and $[Y_s]$ for each data site in view of the initial estimate of the structure with attempts then to achieve agreement.

Principal-axis estimates. The dip axis and principal directions of $[Z]$ are found from the coordinate rotation properties of the tensors in (12). The dip-axis estimates are defined by the x' axis for $\Phi = \Phi_{s0}$, obtained from

$$\Phi_{s0} \rightarrow |Y_{xy}'(\Phi)|_{\max} \tag{13}$$

The higher impedance principal direction of $[Z]$ is defined by the x' axis for $\Phi = \Phi_0$, obtained from

$$\Phi_0 \rightarrow |Z_{xy}'(\Phi) + Z_{yx}'(\Phi)|_{\max} \tag{14}$$

The rotation angles are usually functions of frequency.

For symmetrical geometry, the x' axis defines the vertical plane of symmetry (x' z plane) and the dip axis for the angle Φ_{s0}. The maximum-impedance axis at angle Φ_0 is either along or normal to the dip axis, depending on the conductivities involved.

For nonsymmetrical geometry, the angle Φ_{s0} defined as in (13) responds to an average or pseudo dip axis of the material to which the electromagnetic field measurements are sensitive

$\Phi_{s0}(\omega)$ then tends to describe variations in pseudo dip axis with depth.

Frequency function for determining a one-dimensional model. If for x'-axis rotation angle Φ_0 the diagonal elements of $[Z']$ are normally small, the orthogonal E and H components are essentially related by

$$E_x' \cong Z_{xy}' H_y' \tag{15a}$$

$$E_y' \cong Z_{yx}' H_x' \tag{15b}$$

The impedances in (15) will be called $Z_\parallel$ and $Z_\perp$ for E-field components that are approximately parallel ($E_\parallel$) and perpendicular ($E_\perp$) to the estimated strike direction. The strike direction as used here is defined as the normal to the vertical plane of symmetry. The dip axis lies within the plane of symmetry. For a symmetrical structure, equations 15 become precise equalities and $Z_\parallel$ and $Z_\perp$ become precisely the impedances for E polarizations parallel and normal to the strike, respectively.

Consider a two-dimensional situation. If homogeneous isotropic material surrounds the origin or measuring point, $Z_\parallel$ and $Z_\perp$ become equal in magnitude in the high-frequency limit. As frequency is decreased $Z_\parallel$ and $Z_\perp$ are equal until a lateral inhomogeneity or anisotropy is sensed. The two functions respond differently to an anomaly and will thus begin to split apart. The behavior of these impedances for still lower frequencies must be considered in synthesizing a $\sigma(z)$ model.

$Z_\perp$ tends at first to be less sensitive to material off the z axis. This effect is crudely explained by the fact that, for a secondary (reflected) wave front incident on the origin at some angle θ to the z axis, the influence of the secondary electric field lying within the plane of incidence is proportional to $\cos\theta$. Consequently, $Z_\perp$ tends to have a sensitivity lobe that is directed along the z axis, a property that makes $Z_\perp$ a good locator of a first horizon in conductivity of the structure and probably a good delineator of lateral changes along the dip axis. The influence of a secondary E field normal to the plane of incidence does not have a geometrical factor that depends on θ; thus, $Z_\parallel$ is more sensitive to material off the z axis and tends to respond to some lateral averaging of the conductivity.

As frequency is decreased such that penetra-

$E_\perp$ and $Z_\perp$ remain permanently affected by the nearest anomaly for all lower frequencies; $E_\parallel$ and $Z_\parallel$ are continuous functions along the dip direction and become laterally constant in the low-frequency limit as though the shallower material were homogeneous. $Z_\parallel$ tends to become independent of shallow material in the two-dimensional structure for lower frequency as it would for a one-dimensional structure. It is thus able to represent the effect of deeper material in the structure without accumulative errors due to shallower anomalies. A one-dimensional interpretation of $Z_\parallel(\omega)$ would therefore seem to define a $\sigma(z)$ more nearly approximating the actual conductivity distribution along the z axis. *Patrick* [1969] discusses this point and demonstrates the phenomenon by fitting one-dimensional models to both $Z_\parallel$ and $Z_\perp$, which were computed for two-dimensional structures at various positions along the dip axis. A line of $\sigma(z)$ models produced from $Z_\parallel$ seems to reproduce a reasonable smoothed version of the original structure. $Z_\perp$ models are more in error beyond the first horizon of the structure and reflect lingering effects of a shallow anomaly on low-frequency values of $Z_\perp$; this pattern causes a constant bias if the deeper structure becomes one-dimensional again.

For three-dimensional structures, the arguments set forth above tend to apply as long as departure from two dimensionality is not too severe. Both E-field polarizations $E_\parallel$ and $E_\perp$ will usually retain some distorting effects of shallower anomalies, but $E_\parallel$ will probably be less distorted. In any case, corrections for such effects can be attempted only after some estimate of the structure has been obtained. Severe departure from two dimensionality can cause considerable error in the estimation of a $\sigma(z)$ model, and such a condition can be anticipated when three-dimensionality indicators of $[Z]$ become large. Real geological structures, however, can often be approximated by an assemblage of two-dimensional or symmetrical structures whose effects are sometimes separable (at least qualitatively) in the resulting three-dimensional impedance tensor [*Word et al.*, 1970].

One-dimensional model synthesis. Suppose an impedance function $Z_a(\omega)$, say $Z_\parallel$, has been chosen from $[Z]$ at a given measurement site

such that Z_a beha-

model $\sigma_m(z)$, approximating the conductivity below the site. The next step then is to perform the inversion process:

$$Z_a(\omega) \rightarrow \sigma_m(z) \qquad (16)$$

If Z_a is known for all ω, unique inversion is made possible by the skin-effect phenomenon [*Bailey*, 1970]. In fact, the range on ω need only be such that effective penetration depths encompass the z range of interest in most cases.

The sensitivity of Z_a to a particular portion of $\sigma_m(z)$ and, consequently, the relative importance of that portion of the model as obtained in the inversion process are of considerable interest. The sensitivity is usually a complicated function of $\sigma_m(z)$ and of measurement noise and is difficult, if not impossible, to formulate analytically. Qualitatively, a particular region of the model is reasonably well defined if it produces flux exclusion (i.e., attenuation of the electromagnetic fields in the z direction is rapid compared to the thickness of the region) over some frequency range. It is of some use to implement this rule as follows. Let $\sigma_m(z)$ be of the discrete form in Figure 3, let δ_n be the skin depth in σ_n, and let ω_n denote the frequency for which layer n would become effective in Z_a (i.e., at ω_n the E field at the surface of layer n is about $1/e$ of its value at $z = 0$). Confidence in layer n of the model can be based on the following qualitative rule:

$$d_n > k\delta_n(\omega_n) \rightarrow \text{layer } n \text{ well defined} \qquad (17a)$$

$$d_n < k\delta_n(\omega_n) \rightarrow \text{layer } n \text{ not well defined} \qquad (17b)$$

That k depends on measurement noise is implicit in this rule; $k = 0.75$ to 1.0, determined empirically by the authors, can be used as a rough guideline for present measurement capabilities. Layer n meets condition 17*b* when either d_n or σ_n is small. The layer may still affect the value of Z_a, although one or both of its parameters is not well defined by the inversion.

A closed-form solution for the inversion problem in (16) is not presently available. All methods now used involve iteration of the forward problem to achieve a fit to the frequency function Z_a. Such methods are well covered in the literature [*Cagniard*, 1953; *Wait*, 1962; *Price*, 1962; *Hopkins and Smith*, 1966; *Swift*, 1967; *Patrick*, 1969]. For the layered model in Figure 3, the solution for Z_a can be found from the easily obtainable expression:

$$Z_{n-1} = F(Z_n', \sigma_{n-1}, d_{n-1}) \qquad (18)$$

by iterating up the z axis, on n, beginning with the bottom layer impedance Z_N. Manual fit of the data requires a considerable amount of skill in manipulating the model parameters. *Hopkins and Smith*, [1966] have devised an orderly procedure to accomplish this. *Wu* [1958] and *Patrick* [1969] have written computer programs to achieve automatically a minimum mean square fit to the impedance function by minimizing the function

$$\Psi = \sum_{\omega} \frac{1}{|Z_a|^2} |Z_a - Z_m|^2 \qquad (19)$$

with respect to all model parameters. Z_m is the model impedance. Variables to which Ψ is insensitive can be made constant to eliminate instabilities in the process. The program written by *Patrick* [1969] was used on the results presented in a later section and has proven to be a very useful tool.

It is convenient to define an apparent-resistivity function for use in place of Z_a as

$$\rho_a(\omega) = \frac{1}{\omega\mu} |Z_a(\omega)|^2 \qquad (20)$$

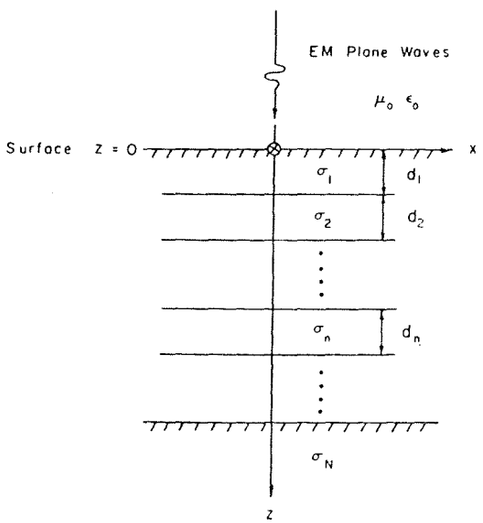

becomes the intrinsic resistivity of the medium. In the one-dimensional model, Z_a behaves as a minimum phase function, and the phase adds no information not contained in ρ_a. Minimum phase behavior seems very apparent in all multidimensional impedance functions measured by the authors, although it is doubtful that such could be expected in every case. The phase of Z_a should certainly be considered in the interpretation.

For a cursory interpretation of an apparent-resistivity function, standard sets of two- or three-layer apparent-resistivity curves [*Cagniard*, 1953; *Yungul*, 1961] can be used for comparison. Also, approximate inversion methods [*Sims*, 1969; *Niblett and Sayn-Wittgenstein*, 1960] have been devised that assume purely exponential decay of the E field in each layer. Such methods are good for mild conductivity contrasts but tend to ignore highly resistive layers.

The initial estimate of subsurface structure formed by an assemblage of one-dimensional models can possibly be refined by considering the behavior of $[Z]$ for individual sites. For example, the estimated dip-axis direction at a particular frequency should be in agreement with the average dip axis of the corresponding portion of the model. Such a comparison provides a good cross check on the results and suggests possible steps for refinement.

A z-ω correspondence is desirable for interpretation of frequency functions such as $\Phi_{zo}(\omega)$. There is no one-to-one correspondence between depth and frequency for a given conductivity function $\sigma_m(z)$; however, an approximate relationship can be established on the basis of a composite skin depth $\bar{\delta}_n(\omega)$ or effective $1/e$ penetration depth into $\sigma_m(z)$ for frequency ω. Let $\bar{\delta}_n$ be defined by

$$\bar{\delta}_n(\omega) = z \qquad |E(z)| = 1/e|E(0)| \qquad (21)$$

The function $\bar{\delta}_n(\omega)$ is monotonic for most probable situations, although it is not precisely so in general (e.g., it would probably not be unique for thick air space between two conductors).

A computer program was written to evaluate $\bar{\delta}_n(\omega)$ and is applied to the results in this study. This depth frequency criterion is perhaps best suited for H_z phenomena because of a tendency source assumed throughout this study, and its existence is an immediate indicator of lateral inhomogeneity. H_z is produced primarily by $H_\perp$ (precisely for two-dimensional cases); consequently, a normalized H_z function defined as

$$H_{zn} \equiv H_z/H_\perp \qquad (22)$$

should be time invariant for a given structure. A map of H_{zn} on an x-$\bar{\delta}_n$ or x-ω cross section tends to locate the position of an anomaly in that plane. Since the secondary wave front producing H_z must propagate from the anomaly, the phase of H_{zn} is advanced or retarded as the measuring point is moved, respectively, toward or away from the anomaly. Insofar as H_{zn} can be associated with a particular anomaly, the 180° directional ambiguity in the dip-axis estimate can be eliminated. In some cases the absolute value of H_{zn} phase seems to indicate whether the anomaly is more conductive or less conductive than the surrounding mediums.

MAGNETOTELLURIC SOUNDING IN CENTRAL TEXAS

Micropulsation measurements were made at seven sites along a 60-mile traverse east of Austin, Texas. Data were taken in the frequency band 0.0001 to 10 Hz, which corresponds to sounding depths ranging from about 0.1 km to over 100 km. Figure 4 shows the traverse on a regional scale along a line bearing approximately N 40°W. Site locations are shown in Figures 5 through 7 on a larger horizontal scale. The site numbers shown were assigned for reference purposes; also, the sites bear the names of nearby landmarks. These names are abbreviated in some figures and they are written out in Table 1. Texas counties are outlined in thin continuous lines in Figures 5 and 6; the MT traverse extends from northern Williamson County through Travis County to southeastern Bastrop County.

Geological background. The MT traverse lies on the flanks of the Llano uplift and crosses the outer portion of the Ouachita fold belt system at the edge of the Texas craton. The Llano Uplift is an exposed crystalline granitic uplift of the Precambrian basement and is associated with the Ouachita system [*Flawn*, 1964; *Woods*, 1956], extending from northern Mexico some

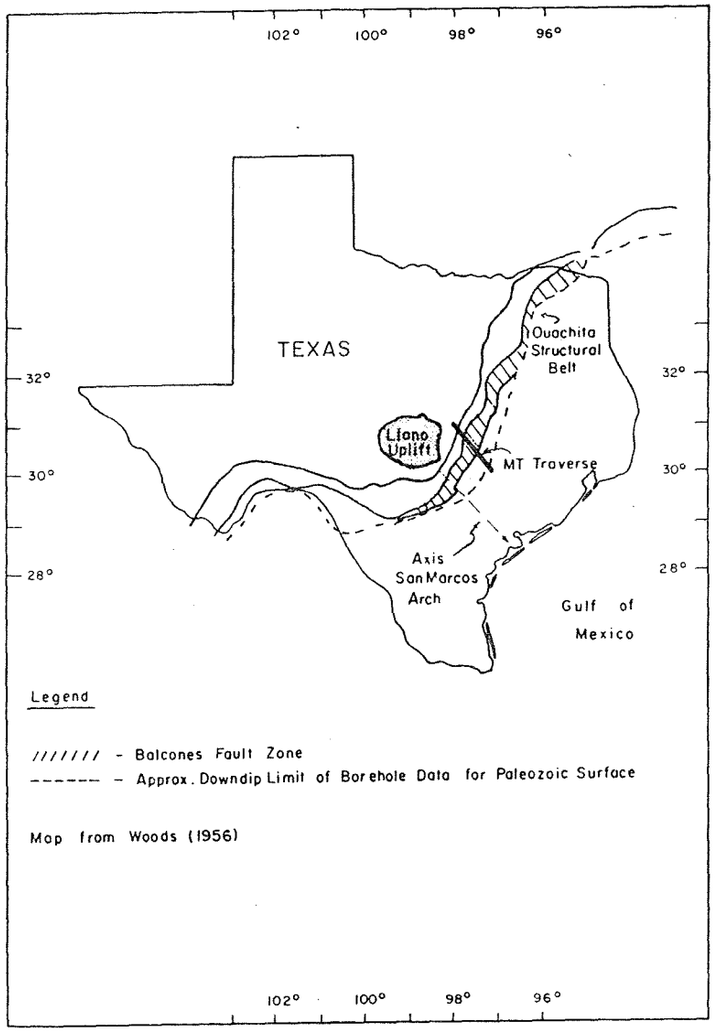

Fig. 4. Magnetotelluric sounding traverse.

The younger sediments overlying the Ouachita system strike about N 20°E near the MT traverse and dip generally southeastward toward the Gulf coast. The Ouachita geosyncline is composed primarily of two structural salients, the east Texas and Rio Grande embayments [*Flawn*, 1964], respectively, separated by the San Marcos arch, whose axis extends from the Llano Uplift outcrop southeast to the coast [*Fowler*, 1956; *Halbouty*, 1966], as shown in Figure 4.

Subsurface geology in the region of the MT traverse is reasonably well known to borehole depths. Borehole penetration to Paleozoic material extends roughly southeast to the broken line in Figure 4. *Flawn et al.* [1961], using nearly all available geophysical evidence, derived a detailed map of the subsurface structure of the Llano uplift and the Ouachita system and provided the information for the contour map of the Paleozoic surface presented in Figure 5. The map in Figure 6 has been redrawn from *Kenney* [1967]. The Precambrian surface contours shown in Figure 6 are based largely on geophysical data and boreholes not reaching the

basement. This surface is not well determined over most of the region shown. Southeast of the zone of overthrust faulting in the Premesozoic, the basement surface depth is beyond reliable estimation; contours are drawn on the Paleozoic or Premesozoic surface south of the fault zone.

Figure 8 is a geological section along the MT traverse; it is derived from various sources including data from maps of the Ouachita structural belt by *Flawn et al.* [1961]. This section shows the various lithologic units along the traverse on a logarithmic depth scale. Since electromagnetic fields tend to attenuate exponentially in the conducting earth, the logarithmic depth scale is a natural one for MT sounding. Paleozoic and Precambrian surfaces were obtained as described above from the contour maps by *Flawn* [1961] and *Kenney* [1967]. The Cretaceous and younger sediments are reasonably well known from borehole penetrations. Contacts between

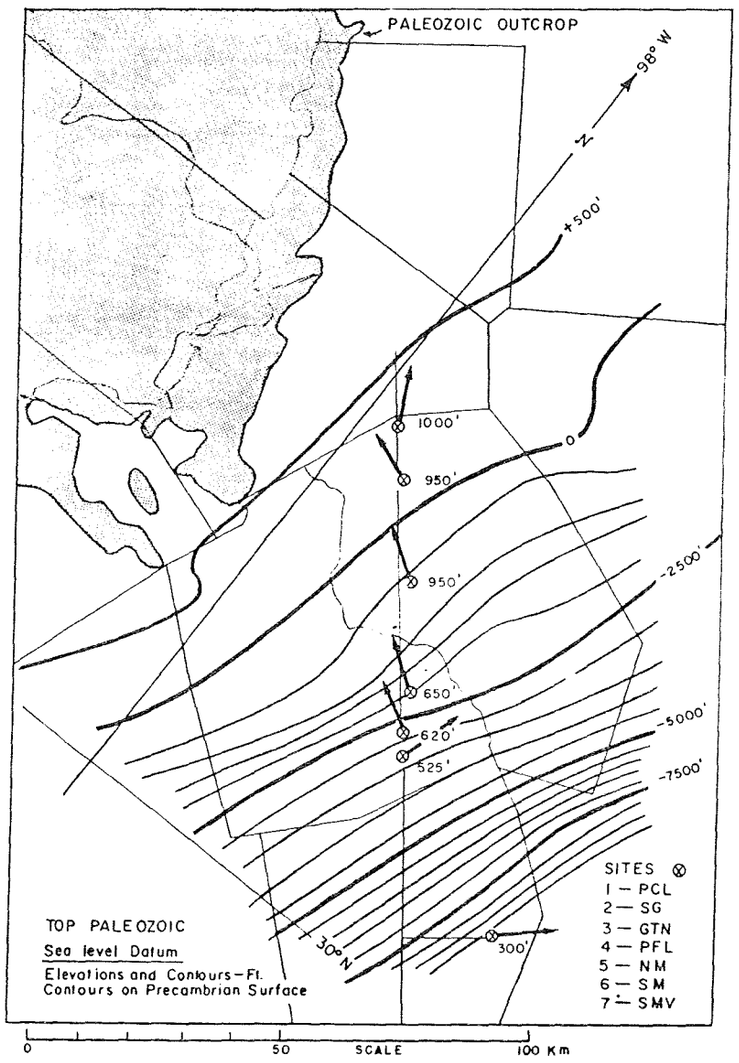

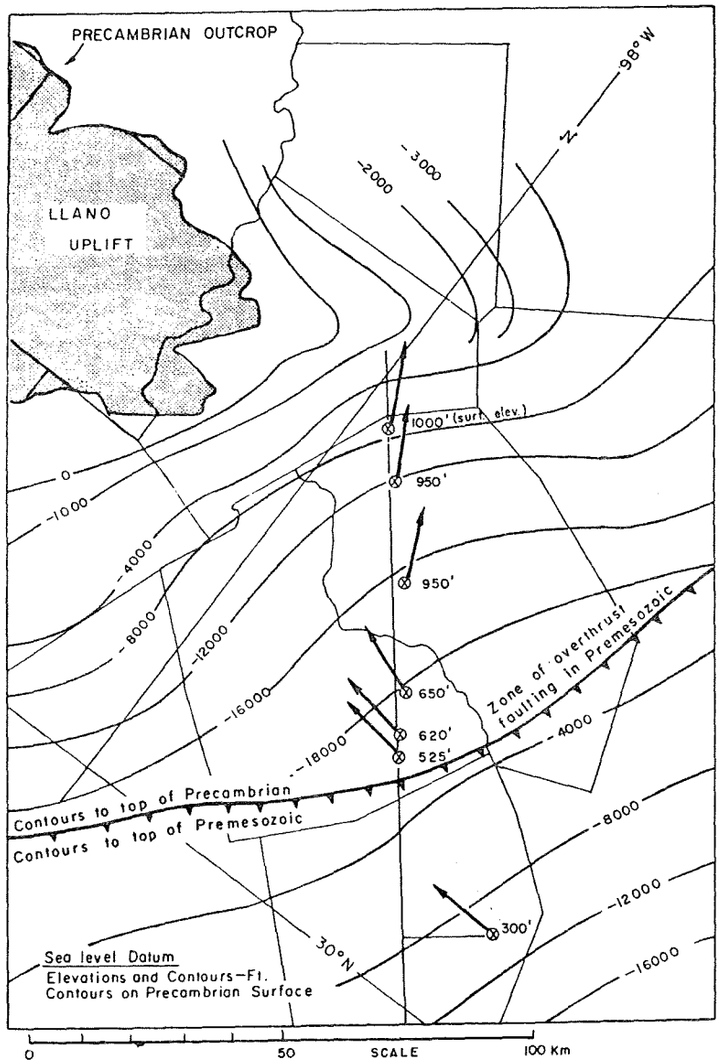

Fig. 6. Rotation angle Φ_{xy} for frequencies sensitive to the Precambrian surface.

the various sedimentary groups seem to be fairly planar, except for occasional normal faulting, and they dip southeastward with a slope of about 0.01. Accurate estimates of contact depths were obtainable near sites 5 and 7. The interfaces, broken lines in the cross section, were drawn with constant slope from known points of surface outcrop through the estimated intersections at sites 5 and 7. Any fault displacements their effect is probably not pronounced, since a good fit with the MT data was obtained with the plane interface assumption. Resistivity logs were available for boreholes designated W1 through W4 at the locations shown in Figure 8. Their resistivity values correlate reasonably well with the broad range of values shown.

Data. Field measurements were made of two components of the electric field (E_x, E_y) and

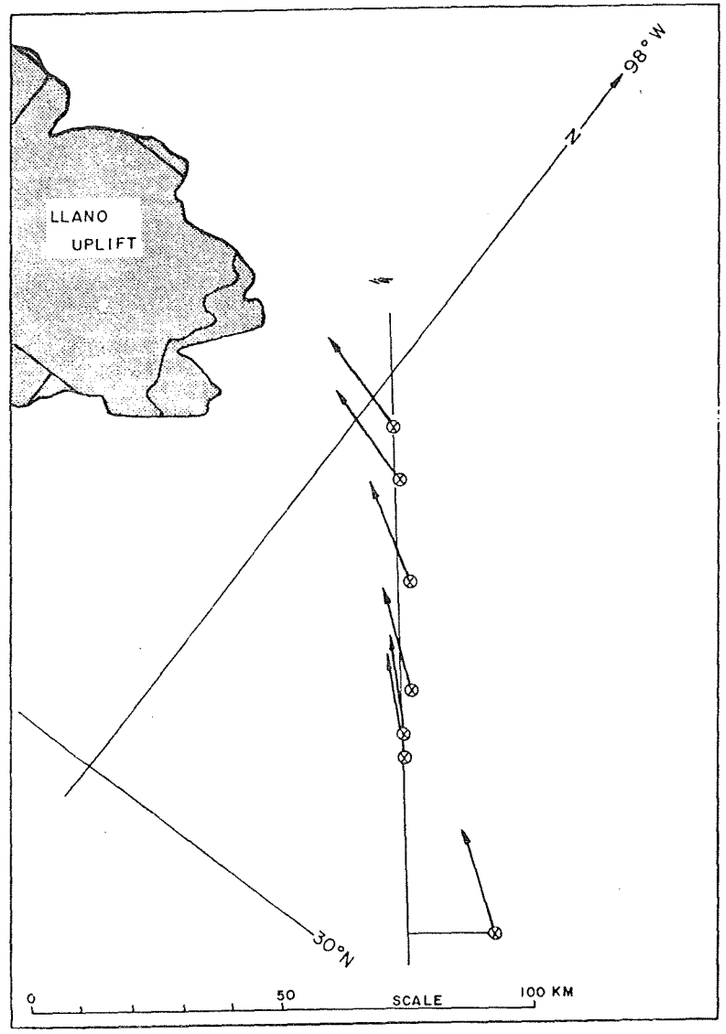

Fig. 7. Rotation angle Φ_{xy} for frequencies sensitive to the conductive substratum.

TABLE 1. Site Designations and Locations

Site No.	Name	Abbrev.	Location	Elev. ft.
1	Purcell	PCL	30°47.88'N, 97°55.48'W	1000
2	San Gabriel	SG	30°42.45'N, 97°52.45'W	950
3	Georgetown	GTN	30°35.25'N, 97°45.88'W	950
4	Pflugerville	PFL	30°27.15'N, 97°35.53'W	650
5	N. Manor	NM	30°22.45'N, 97°31.83'W	620
6	S. Manor	SM	30°20.40'N, 97°32.17'W	525
7	Smithville	SMV	30°02.63'N, 97°08.25'W	300

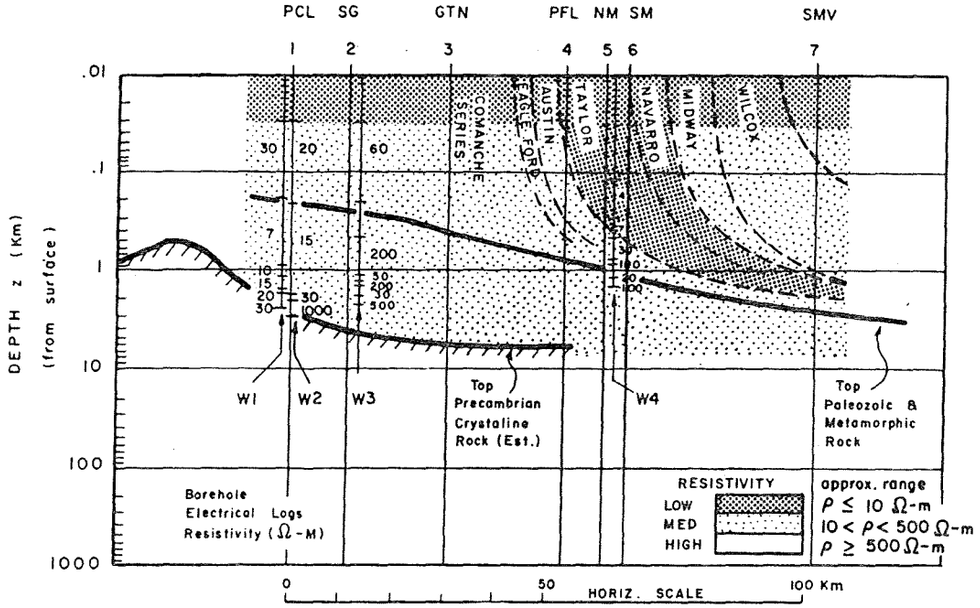

Fig. 8. Geological section along MT traverse with electric log resistivities.

H_z) at each of the seven sites by using the MT instrumentation system developed at the Geomagnetic Laboratory of The University of Texas at Austin [*Word et al.*, 1970]. The frequency range from about 0.0001 to 10 Hz was covered in three overlapping bands (low, medium, high). These were recorded with system responses adjusted to pre-whiten approximately the spectra within each range. An effort was made to obtain at least three good data sequences for each of the three frequency bands; up to six or eight were usually obtained for the medium and high bands. Record lengths averaged about 20 hours for the low band, 2 hours for the medium band, and 15 minutes for the high band.

Data analysis. All data sets were analyzed on a CDC 6600 computer using the techniques described by *Sims* [1969] and *Word* [1970]. Included were the computations of power density spectra, cross spectra, coherency, and polarization from which the following quantities were obtained: apparent resistivity and phase angle for the principal axes of $[Z']$; rotation angles Φ_0 and Φ_∞ for the principal x' axes of $[Z']$ and $[Y']$, respectively; the skew $|s|$; the ellipticity β_0, for the measured impedance $[Z]$, and the ellipticity β_∞ for the measured admittance $[Y_z]$.

RESULTS

A criterion for accepting data points for apparent resistivity and phase angle was based mainly on the phasor coherency as defined by *Sims* [1969]. Only data points having values greater than 0.8 were used in the interpretation. Figure 9 shows a plot of the apparent resistivity and phase versus frequency for the principal elements of $[Z'(\Phi_0)]$ at the North Manor site. The elements $\rho_\parallel$ and $\rho_\perp$ correspond to $E_\parallel$ and $E_\perp$; the continuous curves in this figure show the model fit obtained for the $\rho_\parallel$ case. Similar results were obtained for the other six sites and all curves are graphed on small scales in Figure 10 for convenience in examining them collectively.

A contour plot of $\rho_\parallel$ in a horizontal distance versus frequency plane along the MT traverse is shown in Figure 11. This is actually a plot of the best fit theoretical $\rho_\parallel$ function for the model to be discussed subsequently; however, the theoretical function, appearing as the continuous line in Figures 9 and 10, serves as a reasonable

One-dimensional profiles. A measured impedance function $Z_a(\omega)$ was chosen from each set of results as typified by Figure 9. One-dimensional layered models of the form of Figure 3 were obtained for all sites by two methods. The first method involved a computer visualization routine whereby a model fit was accomplished by successive manual adjustments of the model parameters; the second method used an automatic computer program written by *Patrick* [1969], which minimizes the mean square difference between the measured and model impedance function with respect to all model parameters.

Plots of $\rho(z)$ for layered models satisfying the apparent-resistivity function $\rho_a(\omega)$ are given in Figure 12. The solid line curves represent the profiles to be used in the two-dimensional section and the broken curves are alternate models; the relatively well defined parameters are drawn as thick solid lines. Certain parameters that were not well defined by the inversion were adjusted to probable values still in agreement with the sounding results: a surface layer of $\rho_1 = 5$ Ω-m was used at each site; thin conductive layers were set to 100 Ω-m or 10^4 Ω-m; and at site 1, ρ_2 and d_4 were taken from borehole log W1. The above assumptions were used when required by lack of enough high-frequency data or by insensitivity of the inversion to the value of the parameter in question.

The surface layer thickness d_1 was adjusted to a maximum permissible value when it was not determined by $\rho_1 = 5$ Ω-m. For sites 3 and 4, d_1 is determined by ρ_1; the broken curve is for $\rho_1 = 12$ Ω-m and is a good estimate of the upper limit on ρ_1 and d_1. For highly resistive layers $\rho_n \to \infty$, the layer thickness d_n is determined by the inversion if $d_n \gg \delta_{n+1}(\omega_n)$, where δ_{n+1} is the effective skin depth in the medium below layer n and ω_n is the frequency at which layer n would influence the surface impedance Z_a (see (17)). For small d_n, the layer is effectively transparent. The 10^4 Ω-m layers for sites 3 and 4 are possibly not actually present. The dimensions shown represent upper limits for which these layers are transparent. Admittedly, transparent resistive layers could be placed anywhere in the profile in this manner, and this always represents a potential source of error

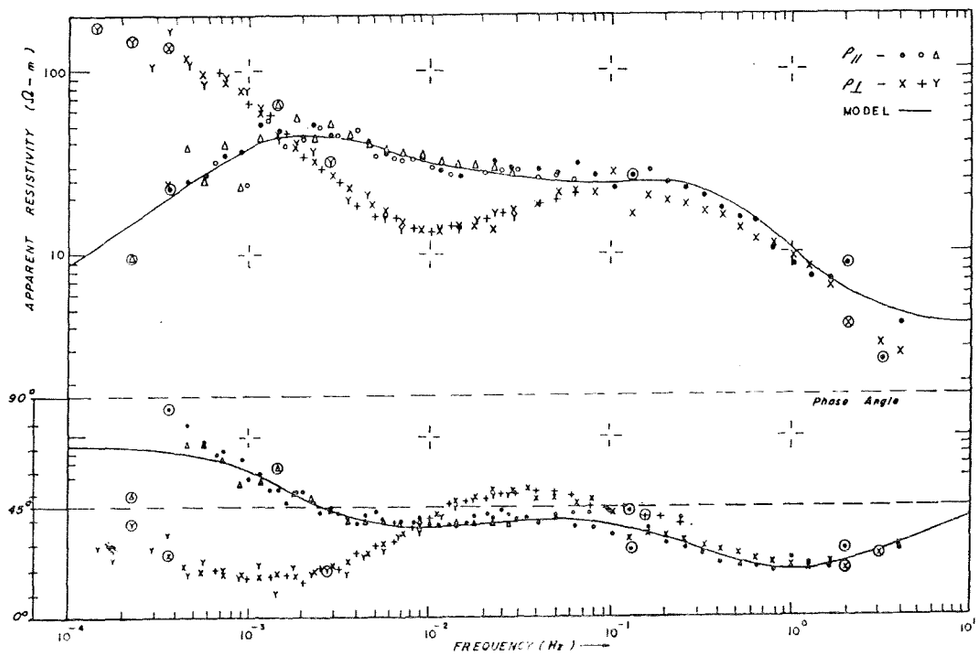

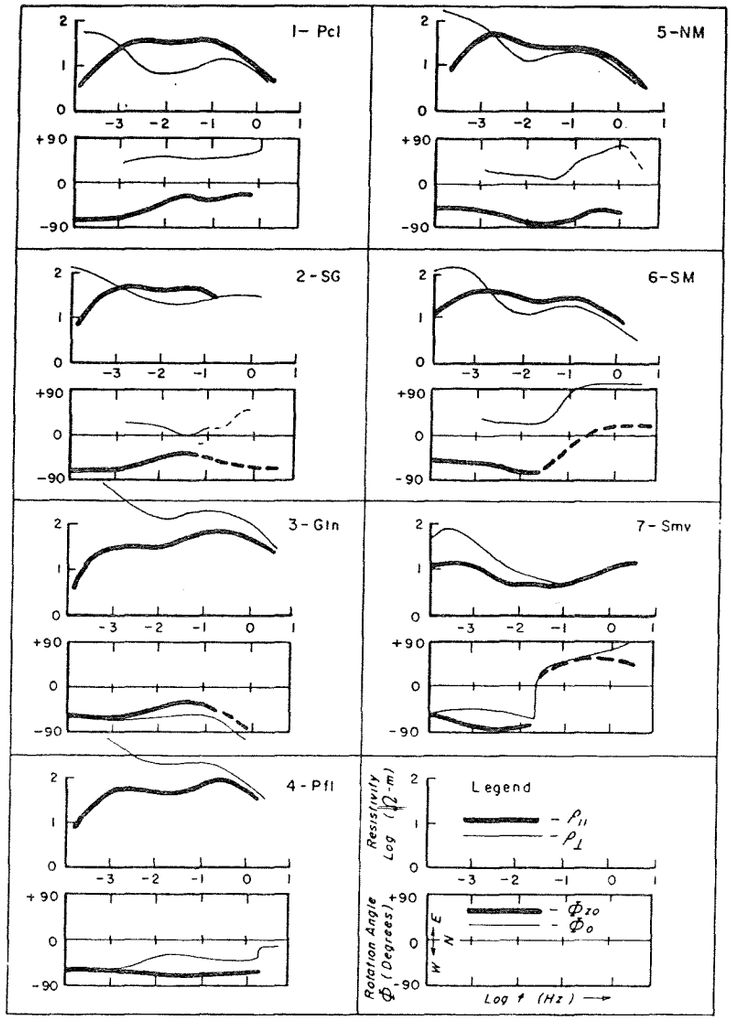

Fig. 10. Summary of apparent resistivity and rotation angle results (see lower right box for legend).

in depth resolution. Nevertheless, when there is reason to expect the presence of a thin resistive region, a useful estimate of the maximum possible thickness can be obtained as above.

For electrically thin and highly conductive layers, only the product $\sigma_n d_n$ is determined by the inversion process; as a result, it is required that a condition such as the setting of thin conductive layers to 1.0 Ω-m be made. Limits could be placed on the values of ρ_n and d_n individually, since the layer would be known electrically thin for the frequencies at which it is effective.

Two-dimensional section. The one-dimensional profile estimates were assembled to produce the vertical cross section shown in Figure 13. Vertical lines represent the data site locations, and the layered model parameters ρ_n and d_n are indicated at each site: the large numerals are layer resistivity in Ω-m and the short cross

$\rho(z)$ for all sites were correlated along the traverse and contoured in 5 resistivity ranges, with interpolation between sites, to form a smoothed estimate of the two-dimensional resistivity distribution. A crude estimate of the horizontal averaging interval along the cross section at a depth z is about $2z$ or less, if a given $\sigma(z)$ is considered influenced by horizontally neighboring material up to a distance z from the measuring site. At a depth of 100 km, the distribution is averaged over the entire traverse at each site.

The relative importance of various features of the model can be gathered from Figure 12. Generally, the shallower portion of the cross section to the first horizon in resistivity is not well defined, owing to lack of adequate high-frequency data; frequencies of up to 10^2 and 10^3 Hz would be needed to obtain good definition for $0.01 < z < 0.1$ km. The high-resistivity bed, marked 10^4 Ω-m, is questionable at sites 3 and 4, and the thickness shown in that region represents an upper limit.

Comparison of model with geology. Comparison of the MT model with the expected geological structure described earlier shows good agreement for most major features of the conductivity distribution, including estimated dip axes. A comparison of the MT profile in Figure 13 with the expected geological section in Figure 8 is facilitated by the superposed sections in Figure 14.

The first horizon in resistivity seen by the sounding is the Austin limestone and lower Cretaceous formation, at sites 1 to 6 and the Wilcox sandstone, at site 7. There is particularly good correlation between the Navarro and Taylor shale beds and the associated conductive streak on the model, which is clearly defined by the sounding at sites 6 and 7.

The Paleozoic surface presents no discernible contrast over the lower Cretaceous and therefore is not defined by the sounding, nor are the various Ouachita facies of the folded Paleozoic material defined, although longer signal averaging in the sounding might detect this material. The lower resistivity regions of the Paleozoic and Cretaceous toward either end of the traverse are possibly associated with different formation facies. The interpolated boundaries between the regions are of course open to question between data sites; however, the geological and electrical boundaries are not expected to conform necessarily. At site 1, near $z = 1$ km, the 8 Ω-m and underlying 100 Ω-m materials prob-

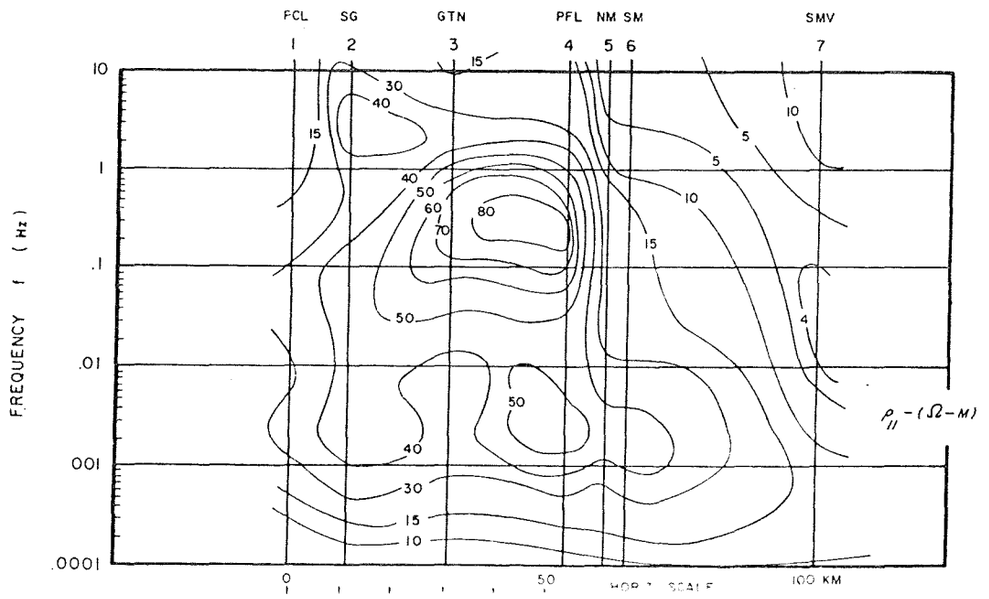

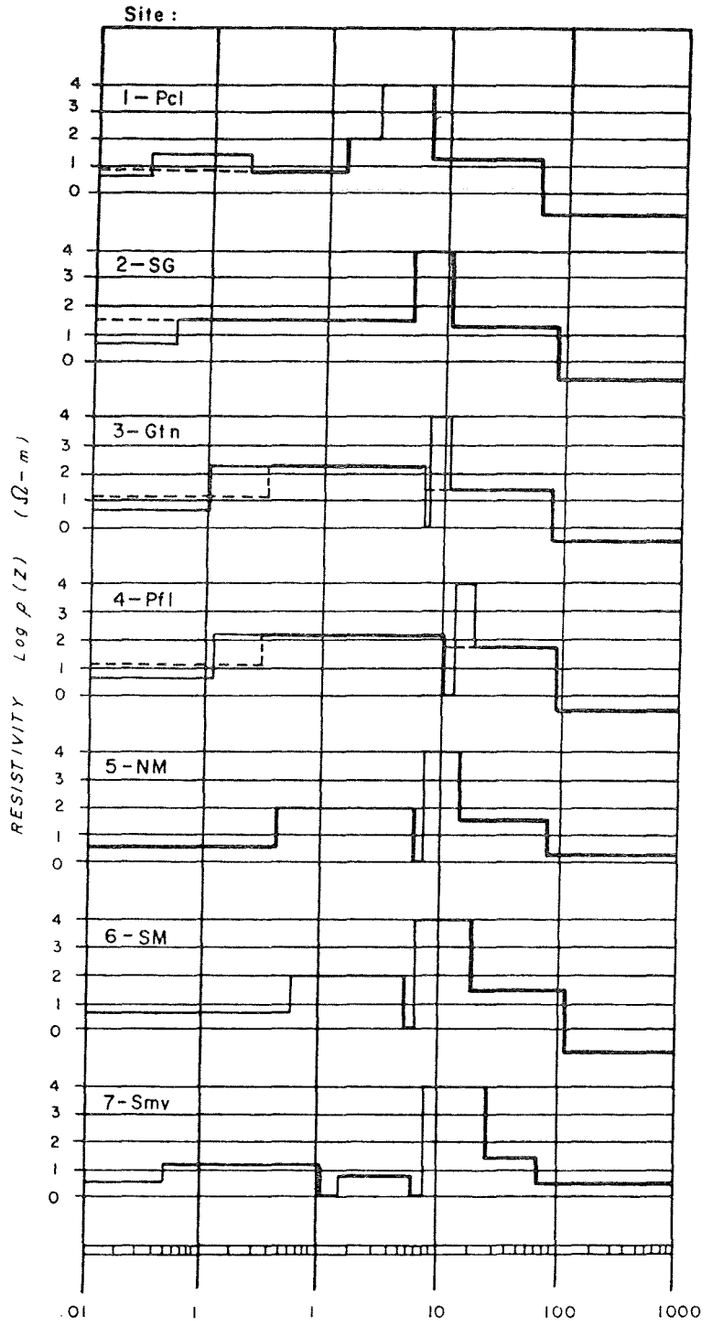

Fig. 12. One-dimensional models.

ably correspond, respectively, to the Upper and Lower Paleozoic rocks of foreland facies.

The resistive bed, 500–∞ Ω-m, is thought to correspond in part to the Precambrian granite basement. The basement surface was detected somewhat deeper than expected at sites 2, 3, and 4. However, discussion with *Flawn* [1961] and other geologists familiar with the Ouachita system would indicate that the model depths are not unreasonable and are within tolerances of the expected surface estimates. The granite is not known to exist over the entire traverse; however, the resistive bed is definitely observed, except possibly between sites 3 and 4.

The thin conductive bed overlying the resistive basement region is found to be a necessary part of the MT model. It may represent a severely weathered granite surface or granite wash. Although a conductive granite surface is not seen at sites 1 and 2, it probably exists but to a lesser extent; the resistivity log for borehole W1 penetrated the granite surface some tens of feet and indicated much lower resistivity than would be expected for granite, i.e., approximately 100–200 Ω-m.

Below the resistive bed, penetration depths are thought to extend into the upper mantle. The lower two conductive layers of the model are a source of concern. The parameters associated with these layers are reasonably well defined in the MT inversion and do not appear to be unduly affected by the influence of noise. However, the indicated resistivity grade-off with depth is much more rapid than is found by deep resistivity soundings in most other areas. *Keller et al.* [1966] show a resistivity-depth distribution compiled from the several methods including, in order of increasing depth, borehole electric logs, galvanic resistivity surveys, magnetotelluric sounding, and studies of long-period magnetic field variations by *Lahiri and Price* [1939] and *McDonald* [1957].

Five major zones of electrical conductivity with depth are recognized by *Keller et al.* [1966] and are labeled A to E from the crust to the core of the earth. Zone A is the surface layer of sedimentary, igneous, and metamorphic rocks. Zone B, probably granite and basalt, is highly resistive, 3×10^3 to 10^5 Ω-m and above. Zone C represents the first significant drop in resistivity for $z \geq 35$ km or so to values found as low as approximately 30 Ω-m, determined by MT in the Colorado Plateau area. Zone D is estimated to begin at $z \approx 200$ km, with further decrease in resistivity. Zone E, the mantle resistivity of 1 Ω-m or less, is estimated to exist for $z \geq 600$ km or so, based on magnetic field variation studies. *Swift* [1967] found a similar conductivity profile with deep MT soundings in Arizona and New Mexico. The low-frequency $\rho_{\parallel}$

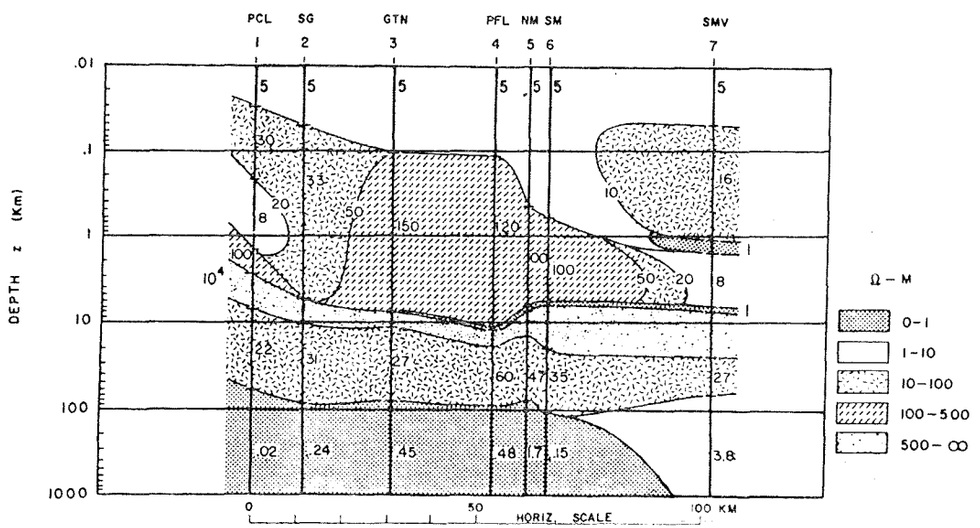

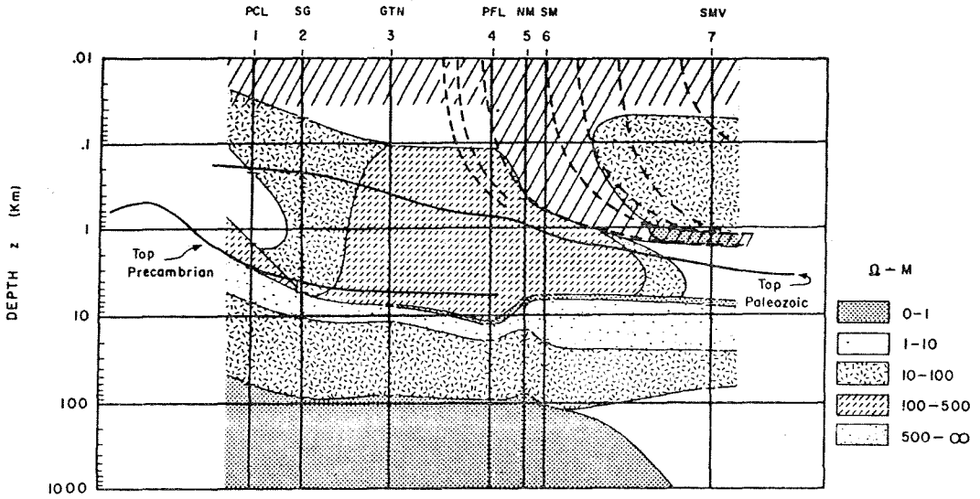

Fig. 14. Superposed geological section.

results in the Swift sounding have a mild decrease with decreasing frequency and are still 15 to 30 Ω-m or so at 10^{-5} Hz, whereas, for the Texas soundings, $\rho_\perp \leq 10$ Ω-m at 10^{-4} Hz and generally the $\rho_\perp$ results have a more rapid decrease with decreasing frequency (see Figures 9 and 10). *Hopkins* [1966] made two MT soundings in the Delaware basin of west Texas at Pecos and Fort Stockton and synthesized layered models to depths in excess of 100 km. The resistivity at Pecos and Fort Stockton was found to decrease to approximately 50 Ω-m at 14.6 and 31 km, respectively, and an ultimate layer of 2.5–10 Ω-m was found at depths of 77 and 106 km, respectively, in reasonable agreement with the results herein.

There is some suggestion of correspondence between the deep (zone *B* and below) resistivity boundaries and seismic boundaries [*Keller et al.*, 1966]; however, there is still insufficient evidence to determine a definite correspondence. According to *Keller* [1966], a decrease in resistivity has been observed at several locations for depth corresponding roughly to the Conrad discontinuity from 10 to 35 km. The resistivity of the basalt or gabbro material below the granite is still placed at over approximately 3000 Ω-m. For the MT section herein, the Conrad discontinuity is possibly within the resistive 500–∞ Ω-m bed. The Mohorovicic discontinuity km [*Cram*, 1962; *Dietz*, 1964] near the Llano uplift is within the conductive region between 10–100 km (see Figure 13).

The deep-resistivity profiles for sites 4, 5, 6, and 7 of Figure 13 are in particularly good agreement with the Hopkins sounding and possibly with the zone *B* and zone *C* transitions of the *Keller* [1966] model. The conductive substrate appears to be about 1/10 as deep as expected, and there is strong evidence of a rise in both conductive substrata toward the northwest.

Dip axes. The principal axis angle Φ_{z0} was used as an estimate of the pseudo dip-axis bearing, to imply the nature of variations off the cross section. Comparison of Φ_{z0} with the expected subsurface contours in Figures 5, 6, and 7 appears to support the speculation that some of the two- and three-dimensional properties of the sounding were attributable to sloping interfaces between formations.

Figure 5 shows the dip axes for a frequency of 1 Hz on the Paleozoic surface contours. The sounding at 1 Hz is thought to be sensitive to material near to and shallower than the Paleozoic surface. It is affected by an area roughly the size of the circles marking the sites in Figure 5 and is expected to be influenced by very local features perhaps at odds with the regional trend. Correlation with the contours in Figure 5 seems quite good, except for sites 1, 6, and 7

formation, which at site 7 possibly has the apparent dip axis shown by the arrow, if we judge by the shape of the surface outcrop.

Figure 6 shows the dip axes on the Precambrian surface contours for frequencies corresponding to the peak in the mid band excursion (rise or dip) in Φ_{z0} for each site. The mid band excursions are confidently attributable to the resistive bed surface.

Figure 7 shows the dip axis for a frequency of 10^{-4} Hz where the sounding is sensitive to the conductive substrate. The tendency for the dip axis to align with the Llano uplift granite outcrop is interesting, particularly in view of the apparent northwesterly rise in the substrate. This pattern would appear to suggest a rise in the conductive mantle associated with the uplift. Additional soundings would be helpful in a study of the nature of the conductive anomaly. A northwest extension of the sounding traverse is planned for the near future.

CONCLUSIONS

In the present study, the conductivity cross section along the central Texas traverse is obtained by contouring the conductivity profiles obtained at each site. Each conductivity profile is obtained by inverting an impedance-versus-frequency function into an estimate of conductivity versus depth. This inverted conductivity estimate is taken to be representative of the true conductivity profile beneath the recording site. Although a quantitative evaluation of the errors involved in constructing such a cross section is quite intractable, it is possible to make a few statements pertaining to the over-all accuracy.

The sensitivity of the MT inversion process to a given earth model parameter is a complicated function of the conductivity structure and the noise influences. Consequently, resolution of the structure will depend on the situation involved, the amount of data available, and the method of interpretation. For a one-dimensional structure, a tolerance of ±10% in depth, thickness, and conductivity is not uncommon for a layer or region meeting the conditions in (17*a*).

The one-dimensional inversions are subject to additional error in the presence of multi-dimensional geology. If the estimates of the impedance tensor give clear evidence of the presence of three-dimensional

derived by one-dimensional inversion. Fortunately, however, all the MT soundings along the central Texas traverse produce impedance tensors that have a strong tendency to diagonalize over a considerable range of frequencies. This feature signals the presence of a nearly two-dimensional earth. In the general case, however, even two-dimensional inversions are almost completely out of the question. If a two-dimensional model were almost completely known, then one or two parameters of that model may possibly be estimated by iterating the numerical evaluation of the almost specified model, but a full two-dimensional evaluation is far too unwieldy. However, the effects of two-dimensional geometry can, to some extent, be accounted for in the one-dimensional treatment by selecting for inversion only that impedance element that is generated by the electric-field component parallel to the strike of the two dimensionality. This strike direction may, of course, be different for structures at different depths beneath the earth's surface. This can be interpreted from the impedance tensor if the angle for which it diagonalizes is distinctly different at different frequencies. In other words, one could interpret a three-dimensional structure if the three dimensionality in fact consists of stacked two dimensionalities whose two-dimensional properties are manifest in the impedance tensor in different portions of the frequency spectrum. In such cases, however, it is necessary to modify the inversion for the deeper of the two structures, because the shallower feature tends to be interactive with the impedance function features of the deeper one.

We conclude that the MT method in its present state of development can become a valuable tool for geophysical exploration if its capabilities are carefully balanced against its limitations.

Acknowledgments. This work was supported by the Office of Naval Research under contract N00014-67-A-0126-0004 and by the National Science Foundation under grant GA 17457.

REFERENCES

Bailey, R. C., Inversion of the geomagnetic induction problem, *Proc. Roy. Soc. London A, 315*, 185–194, 1970.

Bloomquist, M. G., H. W. Smith, F. X. Bostick,

67-0640, Elec. Eng. Res. Lab., Univ. of Texas at Austin, Aug. 1967.

Bostick, F. X., Jr., and H. W. Smith, An analysis of the magnetotelluric method for determining subsurface resistivities. *Rep. 120.* Elec. Eng. Res. Lab., Univ. of Texas at Austin, Feb. 1961.

Bostick, F. X., Jr., and H. W. Smith, Investigation of large-scale inhomogeneities in the earth by the magnetotelluric method, *Proc. IRE, 40*(11), 2339–2346, 1962.

Bryunelli, B. E., Magnetotelluric profiling in conditions of horizontally inhomogeneous media, *Akad. Nauk SSSR Geophys.,* 600–604, 1964.

Cagniard, L., Basic theory of the magnetotelluric method of geophysical prospecting, *Geophysics, 18,* 605–635, 1953.

Cantwell, T., and T. R. Madden, Preliminary report on crustal magnetotelluric measurements, *J. Geophys. Res., 65*(12), 4202–4205, 1960.

Cram, I. H., Crustal structure of Texas coastal plain region, *Bull. Amer. Ass. Petrol. Geol., 46* (9), 1721–1727, 1962.

d'Erceville, I., and G. Kunetz, The effect of a fault on the earth's natural electromagnetic field, *Geophysics, 27*(5), 651–655, 1962.

Dietz, R. S., Origin of continental slopes, *Amer. Sci., 52,* 50–69, 1964.

Flawn, P. T., Basement rocks of the Texas gulf coastal plain, *Trans. Gulf Coast Ass. Geol. Soc., 14,* 281–275, 1964.

Flawn, P. T., A. Goldstein, Jr., P. B. King, and C. E. Weaver, The Ouachita system, *Publ. 6120,* Bur. Econ. Geol., Univ. of Texas, Austin, Oct. 1961.

Fournier, H., La spectrographie directionelle magneto-tellurique a Garchy (Nievre), *Ann. Geophys., 19*(2), 1963.

Fowler, P., Faults and folds of south-central Texas, *Trans. Gulf Coast Ass. Geol. Soc., 6,* 37–42, 1956.

Halbouty, M. T., Stratographic-trap possibilities in upper jurassic rocks, San Marcos arch, Texas, *Bull. Amer. Ass. Petrol. Geol., 50*(1), 3–24, 1966.

Heirtzler, J., A summary of the observed characteristics of geomagnetic micropulsations, in *Natural Electromagnetic Phenomena Below 30 Kc/sec,* edited by D. R. Bleil, pp. 351–372, Plenum, New York, 1964.

Hopkins, G. H., Jr., and H. W. Smith, An investigation of the magnetotelluric method for determining subsurface resistivities, *Rep. 140,* Elec. Eng. Res. Lab., Univ. of Texas, Austin, Feb. 1966.

Keller, G. V., L. A. Anderson, and J. I. Pritchard, Geological survey investigations of the electrical properties of the crust and upper mantle, *Geophysics, 31*(6), 1078–1087, 1966.

Kenney, D. M. (Ed.), Basement map of North America, Amer. Ass. Petrol. Geol. and U.S. Geol. Surv., 1967.

Lahiri, B. N., and A. T. Price, Electromagnetic induction in non-uniform conductors, and the determination of the conductivity of the earth from terrestrial magnetic variations, *Phil. Trans. Roy. Soc. London A, 237,* 509–540, 1939.

Mann, J. E., Jr., Magnetotelluric theory of the sinusoidal interface, *J. Geophys. Res., 69*(16), 3517–3524, 1964.

McDonald, K. L., Penetration of the geomagnetic secular field through a mantle with variable conductivity, *J. Geophys. Res., 62*(1), 117–141, 1957.

McNish, A., The Aurora, in *Natural Electromagnetic Phenomena Below 20 kc/sec,* edited by D. R. Bleil, pp. 77–93, Plenum, New York, 1964.

Niblett, E. R., and C. Sayn-Wittgenstein, Variation of electrical conductivity with depth—the magneto-telluric method, *Geophysics, 25*(5), 998–1008, 1960.

Orange, A. S., and F. X. Bostick, Jr., Magnetotelluric micropulsations at widely separated stations, *J. Geophys. Res., 70*(6), 1407–1414, 1965.

Parkinson, W. D., The influence of continents and oceans on geomagnetic variations, *Geophys. J., 6,* 441–449, 1962.

Patrick, F. W., Magnetotelluric modeling techniques, Ph.D. thesis, Univ. of Texas at Austin, January 1969.

Pokityanksi, I. I., On the application of the magnetotelluric method to anisotropic and inhomogeneous masses, *Bull. Acad. Sci. U.S.S.R., Geophys. Ser.,* 1050, 1961.

Pospeyev, V. I., Some results of magnetotelluric sounding in Irkutsk amphitheater, *Geofiz. Issled., 5,* 94–96, 1965. (translated from Russian by E. R. Hope, Defense Res. Board, Ottawa, Ontario, Sept. 1966.)

Price, A. T., The theory of magnetotelluric methods when the source field is considered, *J. Geophys. Res., 67*(5), 1907–1918, 1962.

Prince, C. E., F. X. Bostick, Jr., and H. W. Smith, A study of the transmission of plane hydromagnetic waves through the upper atmosphere, *Rep. 134,* Elec. Eng. Res. Lab., Univ. of Texas, Austin, July 1964.

Rankin, D., The magnetotelluric effect on a dike, *Geophysics, 27*(5), 666–676, 1962.

Sims, W. E., Methods of magnetotelluric analysis, Ph.D. thesis, Univ. of Texas, Austin, Jan. 1969.

Spitznogle, R. R., Some characteristics of magnetotelluric fields in the Soviet Arctic, Ph.D. thesis, Univ. of Texas, Austin, 1966.

Srivastava, S. P., Method of interpretation of magnetotelluric data when source field is considered, *J. Geophys. Res., 70*(4), 945–954, 1965.

Srivastava, S. P., J. L. Douglass, and S. H. Ward, The application of the magnetotelluric and telluric methods in Central Alberta, *Geophysics, 28,* 426–446, June 1963.

Swift, C. M., Jr., A magnetotelluric investigation of an electrical conductivity anomaly in the southwestern United States, Ph.D. thesis, Geophys. Dep., M.I.T., Cambridge, Mass., July 1967.

Vozoff, K., H. Hasegawa, and R. M. Ellis, Results and limitations of magnetotelluric surveys in simple geologic situations, 1, *Geophysics, 28*(5), 778–792, 1963.

Vozoff, K., R. M. Ellis, and M. D. Burke, Telluric currents and their use in petroleum exploration, *Bull. Amer. Ass. Petrol. Geol., 48*(12), 1890–1901, 1964.

Wait, J. R., On the relation between telluric currents and the earth's magnetic field, *Geophysics, 19*(2), 281–289, 1954.

Wait, J. R., Theory of magneto-telluric field, *Radio Sci., 66D*(5), 509–541, 1962.

Weaver, J. T., The electromagnetic field within a discontinuous conductor with reference to geomagnetic micropulsations near a coastline, *Can. J. Phys., 41,* 484–495, 1963.

Woods, R. D., The northern structural rim of the Gulf basin, *Trans. Gulf Coast Ass. Geol. Soc., 6,* 3–11, 1956.

Word, D. R., H. W. Smith, and F. X. Bostick, Jr., An investigation of the magnetotelluric tensor impedance method, *Tech Rep. 82,* Elec. Geophys. Res. Lab., Elec. Res. Center, Univ. of Texas at Austin, March 1970.

Wu, F. T., The inverse problem of magnetotelluric sounding, *Geophysics, 33*(6), 972–979, 1958.

Yungul, S. H., Magnetotelluric sounding three-layer interpretation curves, *Geophysics, 26*(4), 465–473, 1961.

DISCUSSION

Madden: You showed a conductive zone in the mantle with resistivity less than 1 ohm-m. Were you working at low enough frequency to measure this? Your longest period was about two hours?

Bostick: All we can say is that we were heading into a conductive zone. The absolute value of the conductivity is not well defined.

Porath: I am not against the conductive zone in the mantle, but it appears to come too shallow under the Precambrian uplift.